Lanthanide-doped upconversion materials: emerging applications for photovoltaics and photocatalysis

2014 Nanotechnology 25 482001

(http://iopscience.iop.org/0957-4484/25/48/482001)

IOP Publishing Nanotechnology
Nanotechnology 25 (2014) 482001 (16pp) doi:10.1088/0957-4484/25/48/482001

Topical Review

Lanthanide-doped upconversion materials: emerging applications for photovoltaics and photocatalysis

Weifeng Yang[1], Xiyan Li[2], Dongzhi Chi[1], Hongjie Zhang[3] and Xiaogang Liu[1,2,4]

[1] Institute of Materials Research and Engineering, Agency for Science, Technology and Research (A*STAR), Singapore 117602
[2] Department of Chemistry, National University of Singapore, Singapore 117543
[3] State Key Laboratory of Rare Earth Resource Utilization, Changchun Institute of Applied Chemistry, Changchun, Jilin 130022, People's Republic of China
[4] Center for Functional Materials, NUS (Suzhou) Research Institute, Suzhou, Jiangsu 215123, People's Republic of China

E-mail: hongjie@ciac.ac.cn and chmlx@nus.edu.sg

Received 16 April 2014, revised 31 May 2014
Accepted for publication 16 June 2014
Published 14 November 2014

Abstract

Photovoltaics and photocatalysis are two significant applications of clean and sustainable solar energy, albeit constrained by their inability to harvest the infrared spectrum of solar radiation. Lanthanide-doped materials are particularly promising in this regard, with tunable absorption in the infrared region and the ability to convert the long-wavelength excitation into shorter-wavelength light output through an upconversion process. In this review, we highlight the emerging applications of lanthanide-doped upconversion materials in the areas of photovoltaics and photocatalysis. We attempt to elucidate the fundamental physical principles that govern the energy conversion by the upconversion materials. In addition, we intend to draw attention to recent technologies in upconversion nanomaterials integrated with photovoltaic and photocatalytic devices. This review also provides a useful guide to materials synthesis and optoelectronic device fabrication based on lanthanide-doped upconversion materials.

Keywords: lanthanide, doping, upconversion, nanoparticle, luminescence, photocatalysis, solar cell

(Some figures may appear in colour only in the online journal)

1. Introduction

The rapid growth of energy consumption has accelerated the depletion of the Earth's oil reserve. However, the costs of continuing on our current energy path are steep, as the combustion of fossil fuels results in damage to human health, the environment, and the economy. Worldwide concerns about such issues have significantly shaped current endeavors toward renewable and green energy resources. Photovoltaics and photocatalysis are two mainstream technologies that can meet sustainable development goals through unlimited access to clean solar energy [1, 2]. Photovoltaic cells (also called solar cells) are semiconductor devices that generate electrical power by converting solar radiation directly into electricity by the photovoltaic effect, as illustrated in figure 1(a). Photocatalysis is a chemical reaction between organic species and free radicals generated from photocatalysts upon irradiation with UV–visible or near-infrared (NIR) light. Figure 1(b) illustrates the basic operating principle of photocatalysis based on a semiconductor to generate free radicals (e.g. •OH and $\bullet O_2^-$).

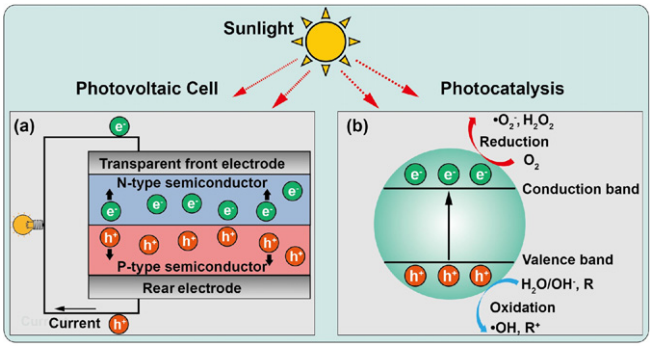

Figure 1. Schematic illustration of the basic principles of (a) a typical solar cell with p-n junction and (b) a typical photocatalytic process based on a semiconductor photocatalyst.

The energy conversion efficiency of current photovoltaic cells is far from satisfactory as they only respond to a relatively small fraction of the solar photons with energy higher than the threshold bandgap (E_g) of the system. This clearly imposes fundamental limitations to the maximum achievable efficiency of solar cells. To boost the conversion efficiency, a nonlinear optical process, known as upconversion, involving lanthanide-doped nanocrystals or thin-film materials, has been recently explored. Lanthanides are the prime candidates to achieve efficient spectral conversion due to their rich energy-level structure that allows for facile photon management [3, 4]. They also have the ability to transform two (or more) sub-bandgap NIR photons into one usable above-bandgap photon, thereby minimizing non-absorption energy losses in photovoltaic devices.

The development of upconversion materials for photovoltaics can be dated back to 1996, when Gibart *et al* [5] reported the application of a 100 μm thick vitroceramic layer co-doped with Er^{3+} and Yb^{3+} on the rear of a GaAs solar cell (figure 2). In the early 2000s, Trupke and Shalav at the University of New South Wales led the pioneering effort on developing the lanthanide-based solar upconverters from theory to practical working devices [6–8]. Another important development was reported by Demopoulos and co-workers, who firstly explored the upconversion effects through the choice of LaF_3:Yb/Er nanocrystals in dye-sensitized solar cells (DSSCs) following AM1.0 G filtered irradiation [9]. In 2011, Wang *et al* demonstrated the feasibility of using commercial LaF_3:Yb/Er upconversion phosphors in P3HT:PCBM organic solar cells [10].

Analogous to photovoltaics, photocatalytic systems having lanthanide-doped materials as spectral converters can operate on the same general principle but with enhanced performance. In 2005, Wang *et al* [11] developed the first visible photocatalyst, based on a combination of Er_2O_3 upconversion materials with TiO_2. To further tap into the potential of NIR light for enhanced photocatalytic reactions, in 2010 Qin *et al* [12] developed a NIR to UV upconversion system comprising TiO_2-coated YF_3:Yb/Tm nanoparticles as the photocatalyst. Another important breakthrough was accomplished by Shi *et al* [13], who reported on an intriguing photocatalyst through use of $SrTiO_3$:Er for visible-light-driven hydrogen production. More recently, Chen *et al* developed ZnO nanorod arrays, decorated with CdTe quantum dots and plasmon-enhanced $NaYF_4$:Yb/Er upconversion nanoparticles, for NIR-driven photoelectrochemical water splitting [14]. These groundbreaking studies have truly revolutionized our understanding of the upconversion principles underlying solar energy conversion processes.

This review aims to give a topical review of the current status of the field of lanthanide-doped upconversion materials, with a particular emphasis on their emerging applications in photovoltaics and photocatalysis. We intend to provide a set of criteria for future work by illustrating the most common designs of solar cells and photocatalysts involving upconversion materials. The success in achieving highly efficient energy conversion will certainly require the expertise of many disciplines, including inorganic synthesis, optoelectronics, catalysis, and materials science and engineering.

2. Photon upconversion in lanthanide-doped materials

2.1. Principles

The fascinating luminescence of lanthanide-doped materials generally arises from electronic transitions within the [Xe]$4f^n$ configuration of the lanthanide dopants [3]. The main intra-4*f* electronic dipole transitions of lanthanide ions are forbidden by quantum mechanical selection rules. Nonetheless, the electronic transitions can be enabled by crystal-field-induced intermixing of the *f* states with higher electronic configurations. Owing to the dipole-forbidden nature of the 4*f*–4*f* transition, these lanthanides exhibit very long decay times in the order of microseconds, which increase the probability of sequential excitations and excited state energy transfer of the lanthanide ions.

Downconversion is a Stokes emission process resulting from an excited lanthanide ion embedded in a host lattice as shown in figure 3(a). In a typical downconversion process, an optical active material absorbs incident irradiation and converts it to lower energy (longer wavelength) photons. Photon upconversion is an anti-Stokes emission process in which the sequential absorption of two or more photons leads to the emission of light at a shorter wavelength than the excitation wavelength. This process was first observed by Auzel in 1966 [15]. Two basic upconversion mechanisms involving lanthanides are excited-state absorption (ESA) and energy transfer upconversion (ETU), as illustrated in figure 3(b). Upconversion can only occur in materials with more than one metastable excited state, in which multiphonon relaxation processes are not predominant. In lanthanides, the electrons at 4*f* or 5*f* sublevels are shielded by the outer 5*s*, 5*p*, 5*d* orbitals and thus they do not strongly participate in the metal-ligand bonding. Consequently, the electron-phonon interaction is reduced and multiphonon relaxation processes are less competitive. Indeed, upconversion is an optical phenomenon most

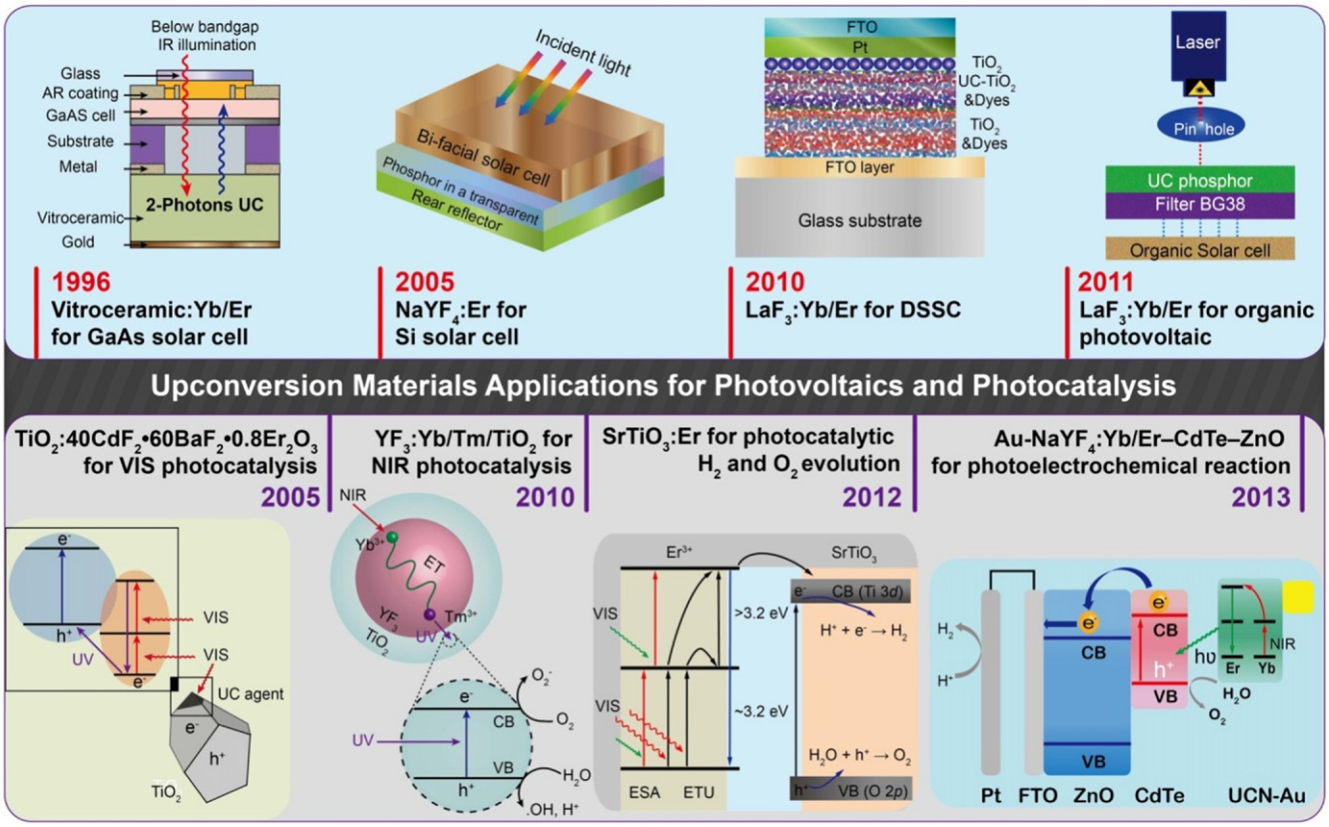

Figure 2. Milestones in the development of lanthanide-doped upconversion materials for photovoltaics (top panel) and photocatalysis (bottom panel). Reproduced with permission from [5, 7, 9–14]. Copyright 1996 IOP Publishing. Copyright 2005 American Institute of Physics. Copyright 2005 Elsevier. Copyright 2010, 2013 The Royal Society of Chemistry. Copyright 2010, 2011, 2012 John Wiley and Sons.

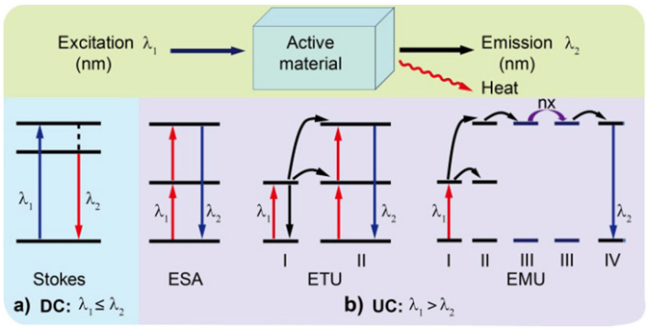

Figure 3. Schematic illustration of downconversion (DC) and upconversion (UC) processes capable of converting λ_1 energy photon input into λ_2 energy photon output. Mechanisms of (a) DC process and (b) UC process: ESA, ETU, and EMU.

commonly observed in materials containing lanthanide ions. Complementary to ESA and ETU processes, our group recently developed energy migration-mediated upconversion (EMU) involving four types of lanthanide ions and a core–shell structure (figure 3(b)) [16]. Through Gd sublattice-mediated energy migration, efficient tunable upconversion emissions in $NaGdF_4$:Tm/Yb@$NaGdF_4$:Ln core–shell nanoparticles were realized for a range of activators (Ln: Eu^{3+}, Tb^{3+}, Dy^{3+} and Sm^{3+}) that do not have long lived intermediary energy states.

2.2. Nanocrystals

Photon upconversion nanocrystals are inorganic nanomaterials that permit the generation of anti-Stokes emission upon excitation with a low-power diode laser (<10 W cm^{-2}). The generation of upconversion luminescence typically requires specific lanthanide activators, singly or multiply doped in crystalline host materials such as halides and oxides [17–20]. Ideal host materials need to have low lattice phonon energies required to minimize non-radiative losses and maximize the radiative emission. Fluorides usually exhibit low phonon energies (~350 cm^{-1}) and high chemical stability, and thus are regarded as the most promising host materials. Er^{3+}, Tm^{3+} and Ho^{3+} ions, featuring ladder-like arrangement energy levels, are frequently doped as activators into the fluoride host lattices to generate upconversion emission under a single NIR wavelength excitation. The amount of the activator needs to be maintained at relatively low level (usually less than 2 mol%) to minimize cross-relaxation energy loss. In most cases, the activator is often co-doped together with Yb^{3+} sensitizer to enhance the upconversion efficiency because of its large absorption cross section at 980 nm.

The development of facile synthetic strategies for high-quality luminescent nanocrystals with controlled crystalline phase, shape and size is crucial to tuning their optical properties and exploring their potential applications in diverse fields. In recent years, a large variety of chemical approaches

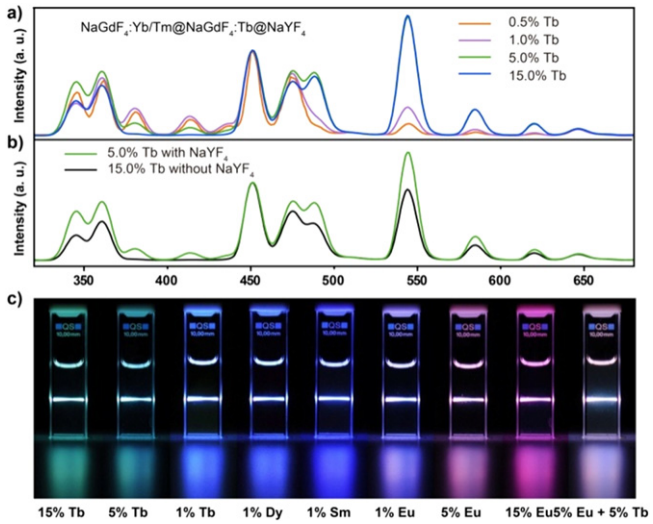

Figure 4. Effect of activator concentration and shell structure on Tb^{3+} emission through Gd sublattice-mediated energy migration. (a) Upconversion emission spectra of the Tb^{3+}-doped $NaGdF_4$:Yb/Tm@$NaGdF_4$:Ln@$NaYF_4$ nanoparticles obtained with different Tb^{3+} concentrations. (b) Comparative spectroscopic studies of the $NaGdF_4$:Yb/Tm@$NaGdF_4$:Tb (15%) with $NaYF_4$-coated $NaGdF_4$:Yb/Tm@$NaGdF_4$:Tb (5%) nanoparticles. (c) Luminescence photographs of representative samples in cyclohexane solution under irradiation of a 980 nm laser. Reproduced with permission from [30]. Copyright 2012 American Chemical Society.

such as thermal decomposition, high-temperature coprecipitation, hydro(solvo)thermal synthesis, sol-gel procedure, cation exchange and ionic liquid-based synthesis have been utilized to synthesize upconversion nanocrystals with well defined size, morphology, absorption and emission profile, carrier lifetime, and surface property [21–29].

Our group recently demonstrated the epitaxial growth of an optically inert $NaYF_4$ layer around a lanthanide-doped $NaGdF_4$@$NaGdF_4$ core–shell nanoparticle for effectively preventing surface quenching of excitation energy [30]. Through Gd sublattice-mediated energy migration, the $NaYF_4$ shell-coating strategy provides tunable upconversion emissions from a variety of activators doped at low concentrations (figure 4). In 2012, Zou *et al* [31] demonstrated a remarkable 3300-fold enhancement in the upconversion luminescence of $NaYF_4$:Yb/Er nanoparticles that are coupled with a cyanine dye (IR-806) to trap photons with energies across a broad range of wavelengths (740–850 nm). The discovery of dye-sensitized upconversion is very important as for the first time, it provides the upconversion emission from lanthanide activators under a broadband and low-power excitation (2 mW). Another notable finding was reported by Qiu's group [32], who demonstrated for the first time the polarized energy transfer upconversion at a single particle level from lanthanide-doped fluoride nanorods. Using a 980 nm linearly polarized laser, the authors observed interesting luminescent phenomena such as sharp energy level split, singlet-to-triplet transitions, and multiple discrete luminescence intensity periodic variation with polarization direction.

More recently, Jin and co-workers revealed that fiber-optic sensors can display sensitivities several orders of magnitude greater than those of existing fluorescent techniques using $NaYF_4$:Yb/Tm upconversion nanocrystals [33]. They found that the integrated emission intensity increases with Tm^{3+} concentration up to 8 mol% without noticeable saturation for a pump power of 2.5×10^6 W cm^{-2}, resulting in a 70-fold emission enhancement. The same group also demonstrated the possibility of generating a library of distinct time-domain codes using $NaYF_4$:Yb/Tm nanocrystals [34]. The ability to precisely control luminescence lifetimes of the upconversion nanocrystals by lanthanide doping provides new opportunities for optical multiplexing in medical research and data security. Another important development was explored by Yu and co-workers, who reported the first demonstration of amplified spontaneous emission and stimulated emission from $NaYbF_4$:Yb/Er@$NaYF_4$ core–shell nanocrystals via two- and three-photon upconversion processes [35]. Their study revealed that the microcavity supports lasing emission for lanthanide-doped nanocrystals through the formation of whispering gallery modes.

2.3. Thin films

The development of optoelectronic devices is largely dependent on advances in thin-film deposition technology. Techniques employed to achieve the deposition of lanthanide-doped upconversion thin films can be broadly classified into chemical vapor deposition and physical vapor deposition, including sputtering [36, 37], pulsed-laser deposition (PLD) [38–42], molecular beam epitaxy (MBE) [43, 44], sol-gel procedure [45–47], thermal evaporation [48], and atomic layer deposition (ALD) [49]. Luminescent materials based on thin films have several advantages over conventional nanocrystals in optoelectronic applications such as excellent thermal stability and outstanding adhesion to solid substrates.

PLD, long known as the tool of choice for the growth of optical materials with a complex stoichiometry, has recently gained increased attention for preparing high-quality lanthanide-doped thin film materials because of its ease of use. The technique of PLD is illustrated in figure 5. A short and high-power (typically ~300 mJ) laser pulse first leads to a rapid removal of material from a solid target housed in an ultrahigh vacuum chamber. The ablated species then form an energetic plasma plume, which then condenses onto a substrate. An example of the principle of using PLD was recently demonstrated by Bubb *et al* [40], who reported the epitaxial growth of single-crystalline $LaEr(MoO_4)_3$ thin films. Upon excitation at 980 nm, the as-grown $LaEr(MoO_4)_3$ thin films emitted light in the visible region as a result of the 4*f*–4*f* transitions of Er^{3+} (figures 6(a) and (b)). Hao *et al* have found a way to modulate upconversion emission using an electric field applied to thin films composed of $BaTiO_3$:Yb/Er (figure 6(c)) [41]. The researchers observed a 2.7-fold enhancement in the green emission band. As the applied voltage increases, the green-to-red intensity ratios were significantly boosted (figure 6(d)).

Another important technique for depositing thin films of upconversion single crystals is MBE, where the deposition rate (typically less than 3000 nm per hour) is precisely controlled to allow the films to grow epitaxially. In 1997, Satoshi

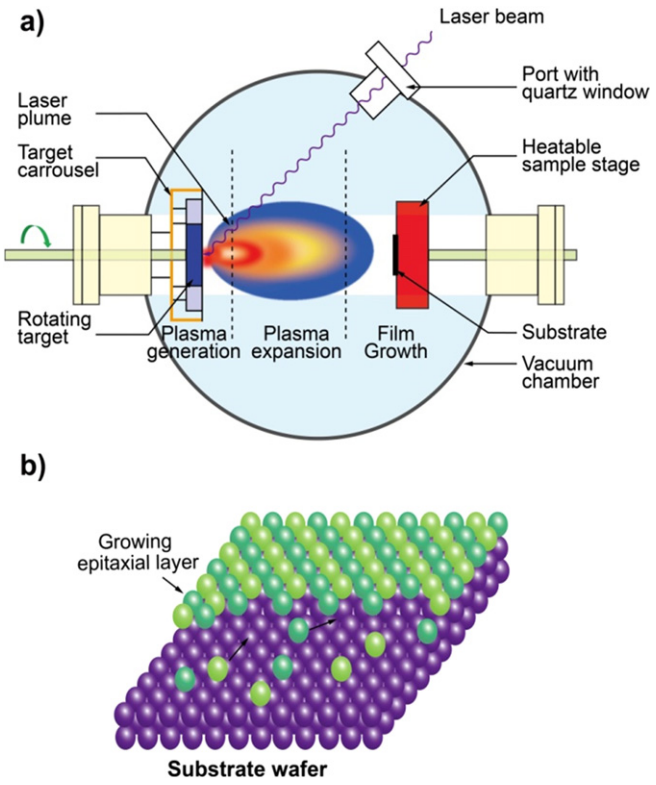

Figure 5. (a) Schematic illustration of a typical PLD system used for the growth of thin films. The deposition process can generally be divided into four stages: laser ablation of the target material and creation of a plasma; plasma expansion dynamics; deposition of the ablation material on a substrate; and nucleation and growth of the film on the substrate. (b) Schematic of the deposition process for metal oxides through layer-by-layer epitaxial growth.

et al [44] reported Er^{3+}-doped LaF_3 upconversion thin films heteroepitaxially grown on CaF_2 (111) substrates by MBE with an Er^{3+} concentration of up to 38.7 mol%. In their study, a maximum emission intensity was obtained with 11 mol% of Er^{3+}. A few years later, Zhang *et al* [43] reported a systematic analysis on the upconversion fluorescence from an Nd^{3+}-doped LaF_3 planar waveguide grown on (111)-oriented CaF_2 substrates by the MBE technique. They found that the cross-relaxation energy transfer processes involving two-photon absorption and three-photon absorption are responsible for the observed upconverted green and orange emissions, and UV emission, respectively. Furthermore, the authors argued that ~1 at% of Nd^{3+} doping content is the optimum concentration required for achieving efficient upconversion in the hetero-epitaxial LaF_3 thin films.

3. Enhancing conversion efficiency in photovoltaics

3.1. Fundamental considerations

The conversion efficiency (η) of a solar cell is a quantitative expression of the balance between the input of solar energy and the measurable energy output in watts [50]. The η is calculated as the ratio between the generated maximum power (P_m) and the incident power (P_{in}). The incident power is equal to the irradiance of AM1.5 spectrum at 25 °C, calculated from the spectral power density $P(\lambda)$ and normalized to 1000 W m^{-2}. In principle, there are two loss mechanisms that contribute to the low energy conversion efficiency of today's solar cells. The first mechanism is the thermalization energy loss in the form of heat dissipation through crystal lattice vibration. The second loss mechanism is ascribed to the non-absorption of photons carrying less energy than the bandgap of the material under investigation. Critically, in the case of crystalline Si (*c*-Si) solar cells, the transmission loss amounts to about 20% of the incident solar energy [51].

Photon upconversion, realized through the use of ladder-like energy levels in lanthanide-doped materials, provides an attractive approach to converting two or more non-absorbed NIR photons into a usable visible photon, potentially enabling the breaking of the Shockley–Queisser efficiency limit for a single junction cell. As illustrated in figure 7, the photons with energy higher than the bandgap of the solar cell can be absorbed, while sub-bandgap photons are transmitted through the device. When an energy upconverter is placed at the back of the solar cell, the transmitted photons can be absorbed by the upconverter. It should be noted that the design of an upconverter in combination with a reflector layer can further boost the energy conversion efficiency of the device. A proof-of-principle demonstration by Trupke *et al* [8] in 2002 showed that the theoretical efficiency limit of a solar cell can reach as high as 63.2% and 47.6% for concentrated and non-concentrated sunlight, respectively. The strategy focusing on the use of upconversion materials for photovoltaics has recently applied to a wide range of solar cells, including those based on Si, GaAs, and dye sensitized materials.

3.2. Dye-sensitized solar cells

Dye-sensitized solar cells (DSSCs) are a new class of efficient photoelectrochemical systems, relying on a semiconductor thin film configured between a photo-sensitized anode and an electrolyte [52]. The emergence of the DSSC has led to next-generation photovoltaics that are color-tunable, transparent, low cost, and flexible. For effective utilization of the solar spectrum, one must consider maximizing the range of energy bands absorbable by the DSSCs. Despite considerable research efforts, the improvement in the efficiency of state-of-the-art DSSCs remains a challenging matter, largely due to the lack of suitable photosensitizers with absorption bands located in the NIR region.

The integration of an upconverter layer into DSSCs may provide a solution. In 2010, Demopoulos and co-workers [9] firstly proposed a multiple-layer structure for enhancing the NIR sunlight harvesting in a conventional DSSC. In their design, LaF_3:Yb/Er phosphors were combined with TiO_2 materials as the upconverter layer to synthesize a triple-layer working electrode. When irradiated at 980 nm (2.5 W), an open-circuit voltage of 0.40 V and a short-circuit current of 0.036 mA were obtained. However, the researchers measured a lowered overall efficiency of the DSSCs, likely due to charge carrier recombination at the interface of the triple-layer

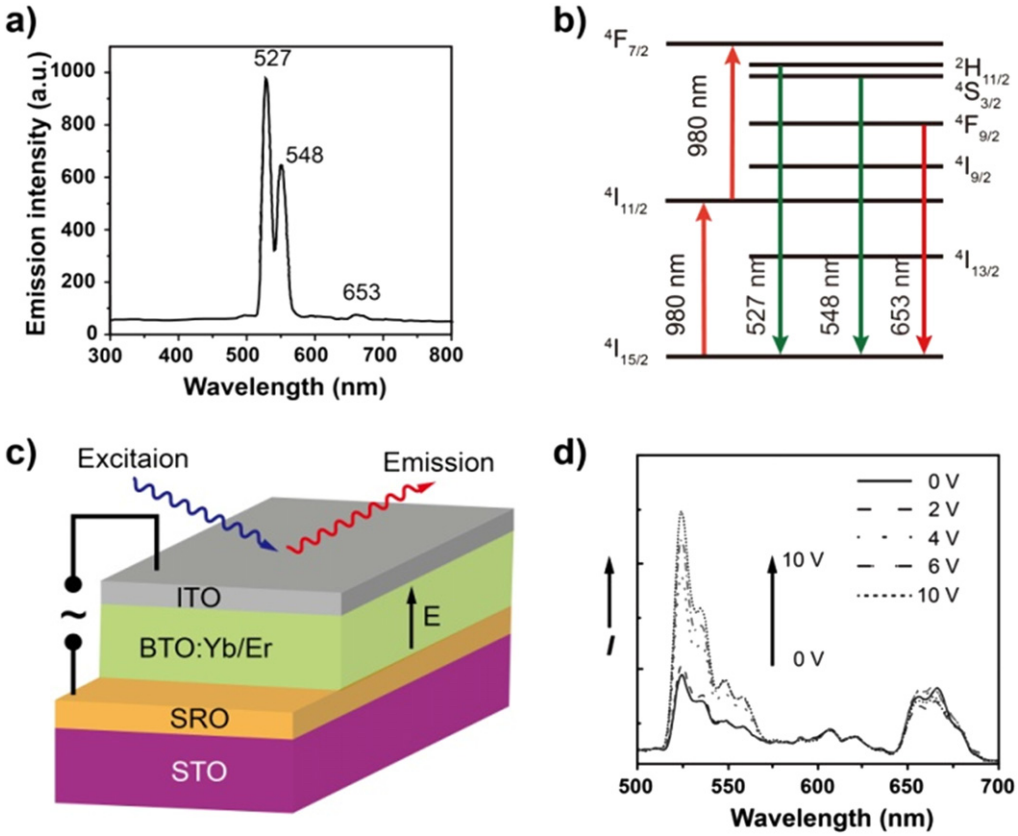

Figure 6. $LaEr(MoO_4)_3$ thin film grown by PLD. (a) Upconversion spectrum obtained using a 980 nm laser. (b) Proposed energy transfer mechanism responsible for the upconversion emission of Er^{3+}. (c) Schematic diagram of electric-field-induced upconversion in a $BaTiO_3$:Yb/Er-based device fabricated by PLD. (d) The corresponding emission spectra obtained under DC bias voltages ranging from 0 to 10 V. Reproduced with permission from [40, 41]. Copyright 2005 American Institute of Physics. Copyright 2011 John Wiley and Sons.

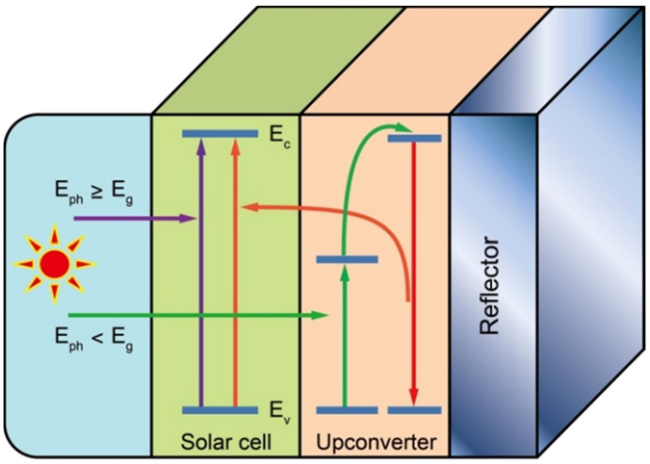

Figure 7. A proposed operating mechanism for a solar cell modified with upconversion materials. Sub-bandgap photons transmitted through the solar cell can be absorbed by the upconverter or reflected by the reflector layer. The upconverting photons with energies matching the bandgap are re-absorbed by the solar cell.

electrode. Shortly after this groundbreaking study, Demopoulos and co-workers further developed a new DSSC configuration comprising highly uniform $NaYF_4$:Er/Yb hexagonal nanoplatelets as an external, bifunctional layer [53]. This arrangement could allow light absorption and reflection to be performed concurrently, thus having advantages in terms of simplified fabrication and enhanced light harvesting. However, both the reflected and upconverted light by the nanophosphors can be absorbed by the electrolyte and the counter electrode used in the external upconversion layer configuration.

In 2013, Liang *et al* [54] reported a nearly 30% efficiency enhancement in DSSCs using core–shell-shell $NaYF_4$:Yb/Er@SiO_2@TiO_2 microplates sandwiched between a counter electrode and a transparent TiO_2 layer in order to take full advantage of the scattering and upconverting functions of the microplates (figure 8(a)). In a parallel investigation, a rear-reflector structure that combines NIR-light-harvesting $NaGdF_4$:Yb/Er/Fe upconversion nanoparticles and light-reflecting silver particles was exploited by Ramasamy *et al* in an effort to improve the performance of the DSSCs (figure 8(b)) [55]. Interestingly, they found that doping of Fe^{3+} ions modified the local crystal field around the Er^{3+} ions, leading to emission enhancement in the $NaGdF_4$:Yb/Er/Fe nanoparticles. An additional 3-fold improvement of the emission intensity was achieved by combining silver particles with the upconversion phosphors, which was predominantly attributed to surface plasmon coupling and large scattering effects of the silver particles.

Another promising system for enhanced light harvesting and conversion was reported by Miao *et al*, who observed

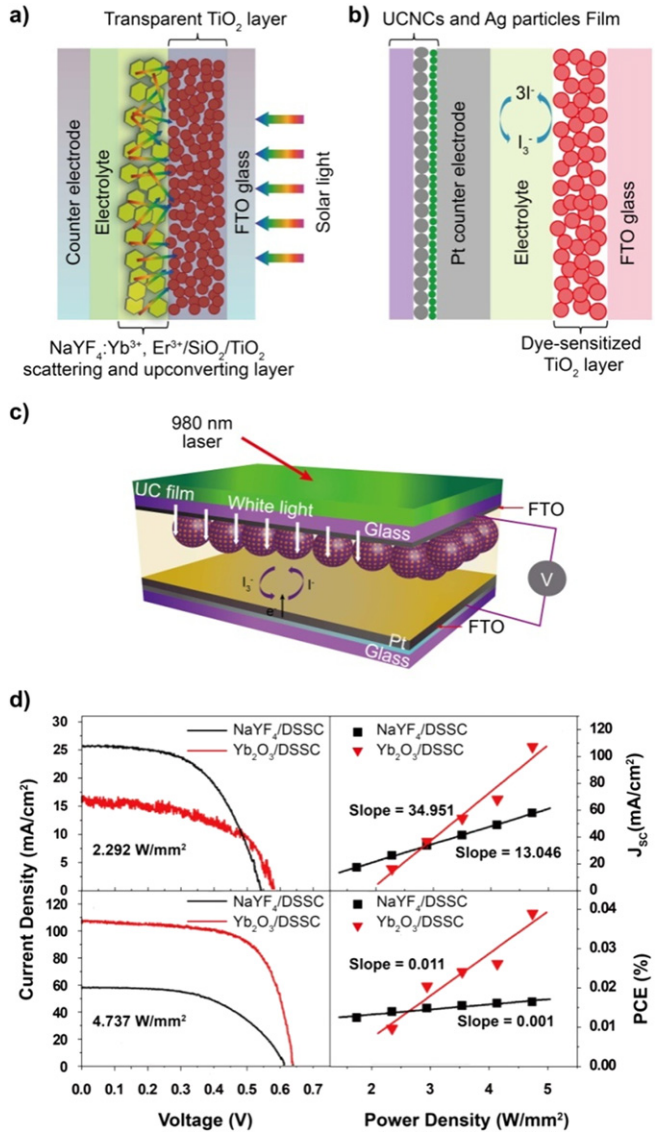

Figure 8. (a)–(c) Schematic diagrams of DSSCs based on β-$NaYF_4$:Yb/Er@SiO_2@TiO_2 microplates, β-$NaGdF_4$:Yb/Er/Fe nanoparticles, and Yb_2O_3 phosphors. (d) Plots of the *J*–*V* curves of Yb_2O_3 and β-$NaYF_4$:Yb/Er DSSCs as well as the laser-to-electrical power conversion efficiency (PCE) and short circuit current densities (J_{SC}) versus 980 nm laser power density. Reproduced with permission from [54–56] Copyright 2013, 2014 The Royal Society of Chemistry. Copyright 2013 Optical Society of America.

super-intense upconverted white emission of Yb_2O_3 polycrystalline powders upon 980 nm excitation [56]. They found that the luminescence intensity of Yb_2O_3 was more than one order stronger than that of well-known β-$NaYF_4$:Yb/Er samples. By arranging the upconversion layer on the front side of DSSCs, the authors observed a much better performance from Yb_2O_3-coupled devices when compared to β-$NaYF_4$:Yb/Er-coupled counterparts (figures 8(c) and (d)). Other upconversion materials, including $Y_3Al_5O_{12}$:Er/Yb transparent ceramics [57], $NaYF_4$:Er/Yb–graphene composites [58] and $TiO_{2-x}F_x$:Er/Yb powder [59], have also been utilized to stretch the absorption of the DSSCs into the NIR region.

3.3. Si-based solar cells

In principle, *c*-Si-based solar cells work best with excitation in the 900–1100 nm range. Therefore, the most desirable upconverters for *c*-Si solar cells are those capable of converting an excitation wavelength of above 1100 nm into an emission at a shorter wavelength centered around 1000 nm. Nanostructured materials doped with Er^{3+} or Ho^{3+} are particularly suitable upconverters for *c*-Si solar cells due to their strong absorption in the NIR region (1480–1580 nm and 1150–1225 nm for Er^{3+} and Ho^{3+}, respectively) and good match of their emission bands (980 nm and 910 nm corresponding to $^4I_{11/2} \rightarrow {}^4I_{15/2}$ transition of Er^{3+} and $^5I_5 \rightarrow {}^5I_8$ transition of Ho^{3+}, respectively) with the absorption of the solar cells.

Shalav *et al* at the University of New South Wales led the pioneering effort to examine the feasibility of using $NaYF_4$:Er (20 mol%) phosphors as the upconverters in a bifacial c-Si solar cell [7]. In their work, reflective white paint was applied to the rear side of the upconversion layer. A peak external quantum efficiency of 2.5% was obtained for the solar cell under excitation by a 1523 nm laser source with 5.1 mW. In 2007, Richards *et al* [60] improved the quantum conversion efficiency to 3.4% using a $NaYF_4$:Er-modified *c*-Si solar cell on excitation at 1523 nm (power density: 2.4 W cm^{-2}). The generation of photocurrent in a commercial *c*-Si solar cell was achieved by Hernández-Rodríguez *et al* in 2013 [61]. In their study, fluoroindate glasses co-doped with Yb^{3+} and Er^{3+} ions were placed on top of the cell, and the incident light is perpendicular to the solar cell and the glass sample (see figure 9(a)). They found that the EQE increases with the power of the source and depends strongly on the concentration of optically active ions in the host material. With an excitation power of 37 mW at 1480 nm, the researchers achieved an EQE of ~0.4% for the Yb^{3+}/Er^{3+} co-doped sample as shown in figure 9(b).

Amorphous silicon (α-Si:H) has a rather large bandgap of 1.7 eV, and its photovoltaic devices thus have higher transmission loss than *c*-Si solar cells. The application of $NaYF_4$:Yb/Er phosphors in α-Si solar cells was first reported by Wild *et al* [62, 63], with a maximum current enhancement of 6.2 μA following illumination at 980 nm (28 mW). This was followed by Chen *et al* [64], who applied a layer of β-$NaYF_4$:Er (10%) microprism coating on the back of a thin film α-Si:H solar cell and investigated its response to sub-band gap NIR excitation (figures 9(c) and (d)). Photocurrents of 0.3 μA and 0.01 μA were obtained for the thin film device illuminated by 980 nm and 1560 nm lasers, respectively. Interestingly, when irradiated with 980 nm (60 mW) and 1560 nm (100 mW) lasers simultaneously, the photocurrent of the device improved to 0.54 μA, indicating that co-excitation with dual wavelengths accessible to upconversion materials is an effective method to enhance the conversion efficiency of photovoltaic devices.

In 2012, Li *et al* reported flexible α-Si:H solar cells made of $NaYF_4$:Yb/Er/Gd (18/2/30%) nanorods and Au nanoparticles [65]. On 980 nm excitation, the authors found that the flexible cell with the upconverters showed a 72-fold

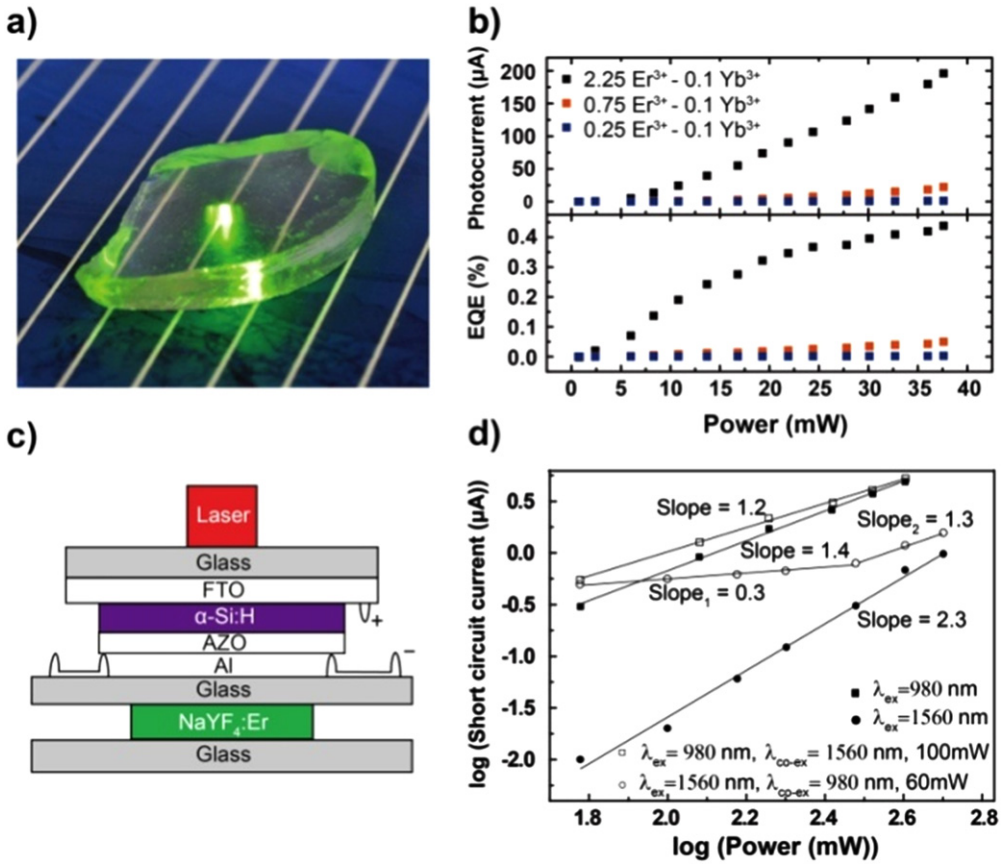

Figure 9. (a) Photograph showing a glass sample co-doped with Er^{3+} and Yb^{3+} placed on a non-bifacial *c*-Si solar cell. (b) Plots of photocurrent and EQE as a function of laser power at 1480 nm. (c) Schematic design of an *α*-Si:H solar cell involving $NaYF_4$:Er microprisms. (d) Log–log plots of short circuit current as a function of excitation power. Reproduced with permission from [61, 64]. Copyright 2012, 2013 Elsevier.

Table 1. Selected photovoltaic devices containing lanthanide-doped upconversion materials.

Solar cell type	Materials	Excitation/Power or power density	Efficiency (Enhancement)	Year [Ref]
GaAs	Vitroceramic:Yb/Er	Ti-Sapphire IR laser/1 W	2.5%	1996 [5]
Organic	$NaYF_4$:Yb/Er	980 nm laser/146 mW	0.0062% (29.1%)	2012 [68]
DSSC	LaF_3:Yb/Er	AM 1.0 solar illumination/100 mW cm^{-2}	2.66%	2010 [9]
DSSC	$NaYF_4$:Yb/Er–graphene	AM 1.5 solar irradiation/100 mW cm^{-2}	2.84% (~4.4%)	2012 [58]
DSSC	$NaYF_4$:Yb/Er@SiO_2	AM 1.5 solar irradiation/100 mW cm^{-2}	8.65% (10.9%)	2013 [71]
DSSC	$TiO_{2-x}F_x$:Yb/Er	AM 1.5 solar irradiation/100 mW cm^{-2}	7.08% (31%)	2013 [59]
DSSC	$NaYF_4$:Yb/Er	AM 1.5 solar irradiation/100 mW cm^{-2}	4.32 (23.1%)	2013 [72]
DSSC	$NaGdF_4$:Yb/Er/Fe	AM 1.5 solar irradiation/100 mW cm^{-2}	7.04% (21.3%)	2014 [55]
DSSC	$NaYF_4$:Yb/Er@SiO_2	AM 1.5 solar irradiation/100 mW cm^{-2}	6.34% (6%)	2014 [73]
c-Si	$NaYF_4$:Er	1523 nm laser/5.1 mW	2.5%	2005 [7]
c-Si	$NaYF_4$:Er	1523 nm laser/6 mW	3.4%	2007 [60]
c-Si	Fluoroindate glass:Yb/Er	1480 nm/37 mW	0.4%	2013 [61]
a-Si	*β*-$NaYF_4$:Yb/Er	980 nm/28 mW	0.03%	2010 [63]
a-Si	$NaYF_4$:Yb/Er/Gd	980 nm /1.1 W	0.14%	2012 [65]

Note: Efficiency is defined as the overall light-to-electrical energy conversion efficiency of the solar cells coupled with upconversion materials. Enhancement refers to the improvement in efficiency when compared to the reference cell without the upconversion materials.

improvement in photocurrent (1.16 mA) and an EQE of 0.14% following an excitation of 1100 mW. More recently, Wild *et al* demonstrated enhanced optical response of *α*-Si:H solar cells for sub-bandgap light under broadband light excitation by utilizing commercially available Gd_2O_2S:Yb/Er-based upconverters [66].

3.4. Other material-based solar cells

Apart from DSSCs and Si-based solar cells, the integration of upconversion materials with other types of solar cells has also been reported, including organic solar cells and GaAs solar cells (table 1). Wang *et al* in 2011 demonstrated for the first

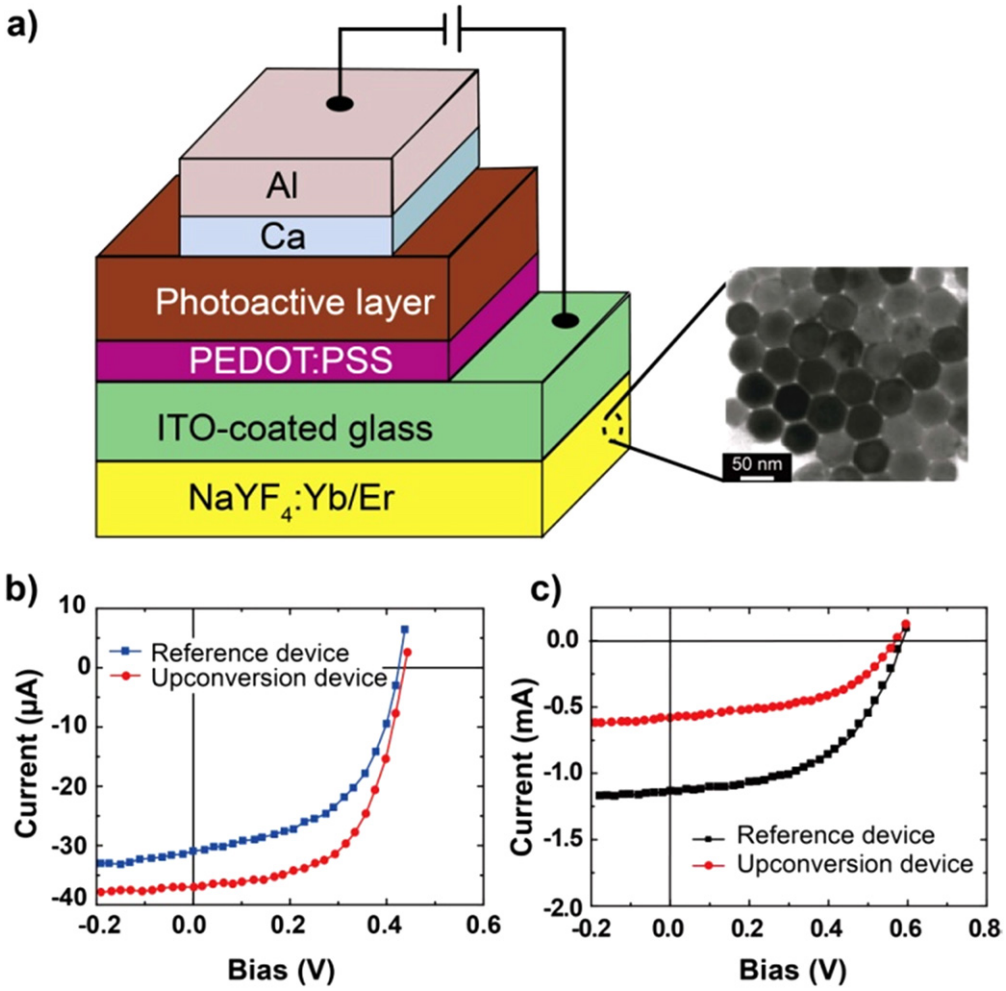

Figure 10. (a) Schematic diagram of an organic solar cell based on $NaYF_4$:Yb/Er phosphors. (Inset) TEM image of the $NaYF_4$:Yb/Er nanocrystals used. (b), (c) *I–V* characteristics of the as-fabricated organic solar cells recorded under illumination with a 980 nm laser at a power of 146 mW and with simulated solar light (AM1.5 G) at 100 mW cm^{-2}, respectively. Reproduced with permission from [68]. Copyright 2012 Elsevier.

time the feasibility of photon upconversion in P3HT:PCBM organic solar cells by LaF_3:Yb/Er phosphors [10]. In their work, a photocurrent density of ~16.5 μA cm^{-2} was obtained on 975 nm excitation (power density: 25 mW cm^{-2}). In a follow-up study, they examined the organic solar cell modified with semiconducting MoO_3:Yb/Er phosphors [67]. The MoO_3:Yb/Er phosphors server as a buffer layer in the solar cell to enable both hole extraction and upconversion capabilities. Upon AM1.5 solar illumination, the researchers obtained less than 1% of the short-circuit current attributable to the upconversion effect.

In 2012, Wu *et al* [68] reported the effects of $NaYF_4$:Yb/Er upconversion nanoparticles on NIR laser-driven polymer solar cells, as illustrated in figure 10(a). The authors observed noticeable enhancements in the photocurrent and efficiency of the solar cells following laser illumination at 980 nm with a power of 146 mW. However, the use of upconversion nanoparticles did not improve the efficiency of the device under illumination with simulated AM1.5 solar irradiation (figures 10(b) and (c)). They suspected that a large portion of the incoming photons was scattered or blocked by the $NaYF_4$:Yb/Er thin film, resulting in decreased performance of the device. Another notable work was reported by Chu and coworkers in 2012 [69], who validated the tantalizing benefit of the upconversion materials by adhering a 300 μm-thick layer of $Y_6W_2O_{15}$:Er/Yb phosphors to the rear of a thin film GaAs solar cell. They obtained a maximum output power of 0.339 μW when illuminated with a 973 nm laser at 145.65 W cm^{-2}.

In 2013, Su *et al* demonstrated an interesting approach for fabricating a hetero-nanostructured photo-anode that comprises $NaYF_4$:Yb/Er@$NaYF_4$ core–shell nanoparticles for enhanced NIR light harvesting [70]. The core–shell approach enables the achievement of spatial confinement of lanthanide activators in the core, thus minimizing surface quenching of upconversion luminescence by solvent molecules. The photo-anode contains an inverse opal featuring a TiO_2 framework filled with quantum dot-modified upconversion nanoparticles. The quantum dots are able to absorb the photons emitted by the upconversion nanoparticles and convert them to electrons. The TiO_2 opal creates a continuous electron conducting pathway and provides a large interfacial

surface area for supporting the upconversion nanoparticles and the quantum dots. As a result, the researchers obtained a much higher electrical current than the control experiment performed on a device without the upconversion nanoparticles.

4. Enhancing photocatalytic performance through broadband absorption

Photocatalysis is an environmentally friendly solution for air or water contamination and soil pollution [74–78]. The photocatalysts in the form of nanoparticles can be dispersed as coatings to building materials for self-cleaning applications. The photocatalytic process is generally initiated by light irradiation of semiconducting materials with band gaps that match the wavelength of the light source. At present, TiO_2, [79, 80] ZnO [81], CdS [82] and Bi_2WO_6 [83] are commonly used photocatalysts for the degradation of organic pollutants. Principally, the photocatalytic activity depends on the ability of the catalyst to generate electron-hole pairs, thus producing hydroxyl radical and superoxide ions. When bound together with harmful pollutants, these highly reactive radicals can effectively oxidize the pollutants and break them down into carbon dioxide and water molecules [84–86].

The photocatalytic performance of a semiconductor material is mainly limited by its intrinsic optical properties as the occurrence of the photocatalytic reaction requires an excitation source with energy equal or greater than the band gap of the semiconductor. For example, titania (TiO_2) is the most frequently used photocatalyst due to its high photostability and low cost, biocompatibility, and chemical inertness. However, TiO_2 with a bandgap of 3.2 eV can only be activated by UV light, a wavelength range which amounts to about 5% usable photons in the solar spectrum [87–89]. To get around this problem, many alternatives have been proposed over the past decade to amplify the photocatalytic activity of TiO_2, either by enhancing the separation of photogenerated charge carriers or making the use of visible radiation feasible. These methods include doping of TiO_2 host lattice with foreign atoms [90, 91], coupling of TiO_2 with organic dyes [92] or quantum dots [93–95], and utilization of upconversion phosphors [12, 96]. In particular, the combination of conventional semiconductor photocatalysts with upconversion phosphors has attracted a great deal of attention by virtue of their unique optical characteristics. By combining luminescent ions (such as Eu^{3+}, Nd^{3+}, Ho^{3+}, Er^{3+}, and Tm^{3+}) with the photocatalysts to form composite materials, high-energy photons in the UV spectral region can be generated by upconverting two or more NIR photons, and subsequently transferred to the photocatalysts (figure 11) [16, 97].

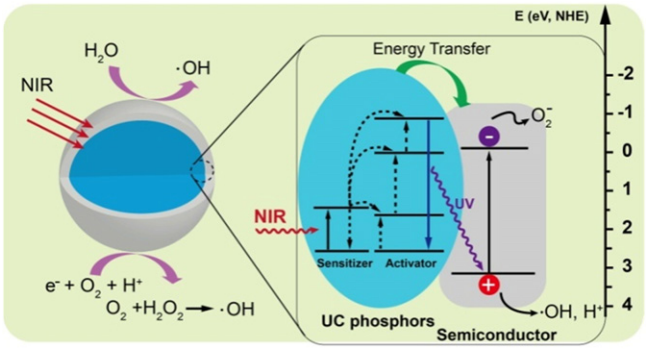

Figure 11. Proposed energy transfer mechanism accounting for enhanced photocatalytic processes in semiconductor catalysts modified with upconversion phosphors.

4.1. Visible-light-active catalysts

For the design and synthesis of photoactive catalysts responsive to visible light, most of the research works have been focused on the use of Er^{3+}-activated composite materials, as Er^{3+} can emit violet light following laser irradiation at a wide range of visible wavelengths (e.g. 450, 488, 542, 633, and 652 nm). In 2005, Wang *et al* combined a composite material of $40CdF_2 \bullet 60BaF_2 \bullet 0.8Er_2O_3$ with TiO_2 to form a hybrid photocatalyst [11]. The researchers observed five emission peaks by this material below 387 nm upon excitation at 488 nm. It is noteworthy that the upconverted emission can be completely absorbed by TiO_2. Their photocatalytic investigations demonstrated that nearly 33% of methylene orange molecules, used as a model organic pollutant, can be degraded within 20 h on 488 nm excitation in the presence of the photocatalyst. By comparison, commercial TiO_2 catalysts only exhibited a maximum degradation yield of 2% under the identical conditions. Since 2005, the use of TiO_2 photocatalysts coupled with upconversion phosphors has been envisaged as an effective approach for the degradation of inorganic and organic pollutants under visible light irradiation [98–100].

Doping by activators, such as Er^{3+} and Tm^{3+}, into semiconductor materials of TiO_2, CdS, $SrTiO_3$, and Bi_2WO_6 presents a promising approach to preparing visible-light-driven catalysts for dye degradation and water splitting. As a proof-of-concept demonstration, Shi *et al* reported the use of Er^{3+}-doped $SrTiO_3$ materials as effective photocatalysts for the generation of H_2 and O_2 molecules following excitation at a broad range of wavelengths [13]. They found that the extended responsive range of the materials from UV to the visible region after Er^{3+} doping was attributed to the generation of elevated excited states of Er^{3+} promoted by the upconversion process and the energy transfer from Er^{3+} to the $SrTiO_3$ host (figure 12). An interesting note is that Er^{3+}-doped $SrTiO_3$ materials with B-site occupancy exhibit higher photocatalytic activity than those with A-site occupancy. Considering the narrow absorption cross section of lanthanide ions, one may consider enhancing the absorption of photocatalytic systems by further integrating them with organic dyes with tunable and high extinction coefficients.

4.2. NIR-light-active catalysts

To explore photoactivation of TiO_2 by NIR light, Yb^{3+}/Tm^{3+} co-doped upconversion nanoparticles can be employed in combination with TiO_2 materials. When photoexcited at

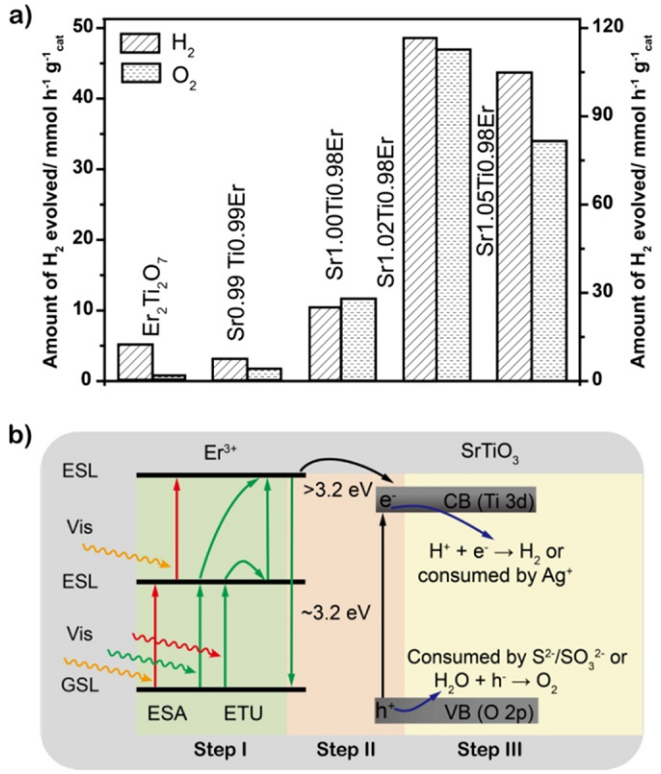

Figure 12. (a) Visible-light-driven photocatalytic effect of different samples on the generation of H_2 and O_2 molecules. The value in *y* axis corresponds to the amount of O_2 evolved during the first 3 h of the reaction and g_{cat}^{-1} represents per gram photocatalyst. (b) Schematic illustration showing the main optical processes of the photocatalytic reaction dominated in the $SrTiO_3$:Er sample. Reproduced with permission from [13]. Copyright 2012 John Wiley and Sons.

980 nm, Yb^{3+}/Tm^{3+} co-doped nanoparticles typically emit two peaks at 290 and 350 nm, resulting from $^1I_6 \rightarrow {}^3H_6$ and $^1I_6 \rightarrow {}^3F_4$ transition of Tm^{3+}, respectively [101]. The production of these two upcoverted UV emissions enables additional electron injection in the conduction band of TiO_2 and facilitates the photocatalytic process, thereby increasing the performance of TiO_2-based materials for photocatalysis using solar irradiation.

In 2010, Qin and co-workers [12] showed that by using TiO_2-coated YF_3:Yb/Tm nanocrystals, photocatalytic activity can be improved. When coated with a layer of TiO_2, the emission intensities of Tm^{3+} at 290 and 350 nm were significantly suppressed, implying the facile energy transfer from the upconversion core to the TiO_2 shell. The use of these hybrid nanocrystals led to an about 61% photodegradation of methylene blue molecules on 980 nm laser irradiation for 30 h, while the controls using pure TiO_2 materials did not show discernable photocatalytic activity under the same experimental conditions. In their recent work, YF_3 host material was replaced by hexagonal phase $NaYF_4$ in order to generate more efficient NIR-light-active photocatalysts [102]. The efficiency in the degradation of methylene blue molecules by the core–shell photocatalysts was improved to ~65% after 14 h of irradiation. Mechanistic investigation on the NIR-light-driven photodegradation of methylene blue molecules by the $NaYF_4$:Yb/Tm@TiO_2 catalyst revealed that the degradation of these organic pollutants can be related to the oxidation of reactive oxygen species rather than to the thermal energy generated by NIR irradiation. In addition to lanthanide-doped $NaYF_4$ and YF_3 host lattices, CaF_2 host matrix has proven effective for use as a co-catalyst in conjunction with semiconductors for the removal of organic pollutants [103]. Similarly, a variety of non-TiO_2-based systems such as CdS [104] and Fe_2O_3 [105], have been explored as promising NIR photocatalysts, combined with upconversion nanomaterials.

The design of unique nanostructures capable of facilitating the energy transfer between the light-upconverting component and the constituent semiconductor catalysts is beneficial to vastly increased photocatalytic efficiency. As the interfacial layer formed between the upconversion and semiconductor materials provide effective control over the current density of the photocatalytic system, the resulting heterojunction should be dense and thin. An innovative strategy was recently reported by Li *et al* [106], who demonstrated the preparation of highly ordered mesoporous TiO_2 nanostructures in the presence of Yb^{3+} and Tm^{3+} ions. The as-prepared TiO_2 nanocrystals were utilized as effective photocatalysts for the degradation of rhodamine B. The mesoporous structure provided a large surface area (113 $m^2\ g^{-1}$) where the solar energy can be adequately harvested to generate oxidative species needed for the redox reaction with pollutants. Another notable example was reported by Zhang *et al* [107], who synthesized $NaYF_4$:Yb/Tm@TiO_2 core–shell microrods by a hydrothermal method. The anatase-phase TiO_2 shell was conformally coated onto the lanthanide-doped $NaYF_4$ microrods with controlled thickness. In the presence of these core–shell microrods, almost 90% of methylene blue molecules were degraded upon NIR irradiation for 12 h.

Alternatively, upconversion nanoparticles can be deposited directly on a semiconductor film to modulate the rate of photocatalytic reactions as in the case of the $NaYF_4$:Yb/Er–hematite film system reported by Liu and co-workers [105]. When excited at 980 nm with a diode laser, $NaYF_4$:Yb/Er nanoparticles, electrochemically deposited on a fluorine-doped tin oxide electrode, emitted at 550 and 670 nm. Subsequently, the upconverted visible photons were absorbed by the surrounding hematite film, leading to a better efficiency in water splitting than conventional hematite materials.

The preparation of photocatalytic systems with prolonged lifetimes of charge carriers for increased photocatalytic efficiency remains a daunting challenge. In most photocatalysts, photogenerated electrons and holes tend to quickly recombine to form electron-hole pairs, thus suppressing the catalytic reactivity of the photocatalysts. An intriguing solution to this problem is to consolidate graphene sheets with the catalytic structures. The graphene sheets are excellent conductors capable of facilitating electron transfer and stabilizing the photogenerated electrons and holes upon NIR light irradiation. In 2012, Ren *et al* [108] demonstrated the degradation of methylene orange molecules by a three-component

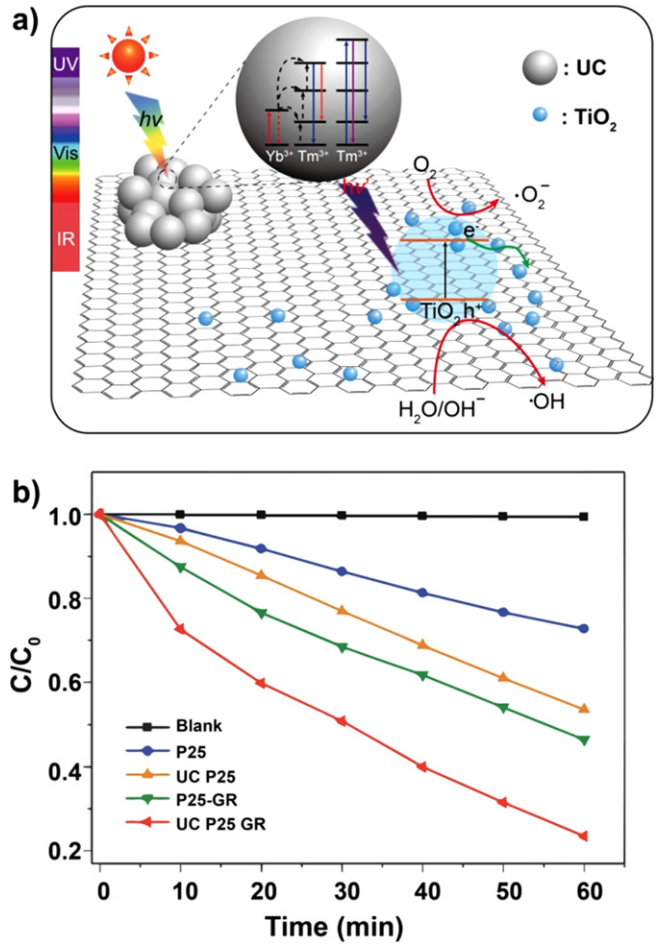

Figure 13. (a) Schematic representation showing a photocatalytic system based on reduced graphene-oxide sheets, commercially available P25 photocatalyst and $NaYF_4$:Yb/Tm nanoparticles. (b) Comparative analysis of photocatalytic performance for the degradation of methylene orange molecules by different photocatalysts. The analytical data was collected from reactions carried out over 60 min and under irradiation of simulated sunlight [108]. Copyright 2010 The Royal Society of Chemistry.

photocatalyst comprising a commercial P25 catalyst, reduced graphene-oxide sheets and $NaYF_4$:Yb/Tm nanocrystals (figure 13). Approximately 30% of methylene orange molecules were decomposed after 10 min when irradiated with simulated sunlight (AM1.5 G) at 100 mW cm^{-2}; this compared with only 4% yield of the decomposition reaction using the P25 photocatalyst alone.

To inhibit the recombination of the photogenerated charge carriers, one may consider enhancing interfacial charge transfer through use of multi-component systems. For instance, Chen *et al* reported a highly efficient water-splitting system, based on a novel photocatalyst involving ZnO nanorod arrays, CdTe quantum dots, and Au nanoparticle-modified $NaYF_4$:Yb/Er nanoparticles [14]. When irradiated at 980 nm, the upconverted visible photons emitted by the $NaYF_4$:Yb/Er nanoparticles were absorbed by the CdTe quantum dots, resulting in the formation of electrons at the conduction band and holes at the valence band. The electrons at the excited states were then transferred to the conduction band of the ZnO nanorod, effectively preventing the recombination of the electrons and the holes. In addition, the authors argued that the modification of the $NaYF_4$:Yb/Er nanoparticles with an optimal amount of Au nanoparticles increased upconversion emission intensity, enabling them to boost the photocurrent density in the photoelectrochemical reaction. The four-component system can provide a short-circuit photocurrent density of up to 0.036 mA cm^{-2} with an applied voltage of 1.0 V, which presents an almost 40-fold improvement over photoelectrodes made of pristine ZnO nanorods. On two parallel investigations, multi-component $YAlO_3$:Er–ZnO–TiO_2 and $NaYF_4$:Yb/Tm@CdS@TiO_2 materials were reported to show improved photocatalytic efficiencies in the degradation of acid red B and methylene blue, respectively [109, 110]. Taken together, these efforts suggest that synergistic material combinations can lead to unprecedented optical properties, which are hardly accessible by an individual constituent.

5. Outlook and perspective

The applications of lanthanide-doped upconversion materials for photovoltaics and photocatalysis are emerging fields with many possibilities and challenges that lay ahead. The upconversion materials have shown great promise in enhancing the optical response of photovoltaic devices and photocatalysts to a wide solar spectrum. Despite the benefit, efficient upconversion processes are generally restricted to Er^{3+}, Tm^{3+}, and Ho^{3+} activators, characterized by ladder-like arranged energy levels. Furthermore, the upconversion materials respond well only to two narrow excitation bands, namely 800 and 980 nm. The realization of efficient upconversion also requires laser irradiation or concentrated sunlight, which clearly hinders the practical implementation of upconversion materials for solar energy harvesting and photocatalysis.

Recent efforts on the investigations of surface plasmon coupling, photonic crystal engineering, and energy clustering at sublattice levels have led to the development of promising approaches to boost upconversion efficiency [19, 111–114]. A long-term goal would involve developing upconversion nanocrystals that can be excited across a broad range of wavelengths [115–118]. Many transition metals, quantum dots, and organic dyes are known to have large absorption cross sections. In this respect, the coupling of highly light-sensitive materials with the upconversion nanocrystals to dramatically improve upconversion luminescence appears feasible. However, for these conjugated systems, the fundamental question of how the transfer of energy occurs between the upconversion nanocrystals and the sensitizers remains unresolved. Finding answers to this question certainly requires considerable, multidisciplinary efforts.

Acknowledgments

X.L. acknowledges the National Research Foundation and the Economic Development Board (Singapore-Peking-Oxford Research Enterprise, COY-15-EWI-RCFSA/N197-1), the Ministry of Education (MOE2010-T2-1-083), and the Agency for Science, Technology and Research (A*STAR) (IMRE/12-8C0101) for providing support during the time this Review was written. H.Z. acknowledges the National Natural Science Foundation of China (Grant Nos. 91122030 and 21210001), and National Natural Science Foundation for Creative Research Group (Grant No. 21221061) for the funding support.

References

[1] Licht S, Hodes G, Tenne R and Manassen J 1987 A light-variation insensitive high efficiency solar cell *Nature* **326** 863–4
[2] Manassen J, Cahen D, Hodes G and Sofer A 1976 Electrochemical, solid state, photochemical and technological aspects of photoelectrochemical energy converters *Nature* **263** 97–100
[3] Auzel F 2004 Upconversion and anti-Stokes processes with f and d ions in solids *Chem. Rev.* **104** 139–74
[4] Wang F and Liu X 2009 Recent advances in the chemistry of lanthanide-doped upconversion nanocrystals *Chem. Soc. Rev.* **38** 976–89
[5] Gibart P, Auzel F, Guillaume J-C and Zahraman K 1996 Below brand-gap IR response of substrate-free GaAs solar cells using two-photon up-conversion *Jpn. J. Appl. Phys.* **35** 4401–2
[6] Shalav A, Richards B S and Green M A 2007 Luminescent layers for enhanced silicon solar cell performance: up-conversion *Sol. Energ. Mat. Sol.* C **91** 829–42
[7] Shalav A, Richards B S, Trupke T, Krämer K W and Güdel H U 2005 Application of $NaYF_4$:Er^{3+} up-converting phosphors for enhanced near-infrared silicon solar cell response *Appl. Phys. Lett.* **86** 013505
[8] Trupke T, Green M A and Würfel P 2002 Improving solar cell efficiencies by up-conversion of sub-band-gap light *J. Appl. Phys.* **92** 4117–22
[9] Shan G B and Demopoulos G P 2010 Near-infrared sunlight harvesting in dye-sensitized solar cells via the insertion of an upconverter-TiO_2 nanocomposite layer *Adv. Mater.* **22** 4373–7
[10] Wang H-Q, Batentschuk M, Osvet A, Pinna L and Brabec C J 2011 Rare-Earth ion doped up-conversion materials for photovoltaic applications *Adv. Mater.* **23** 2675–80
[11] Wang J, Wen F, Zhang Z, Zhang X, Pan Z, Zhang L, Wang L, Xu L, Kang P and Zhang P 2005 Degradation of dyestuff wastewater using visible light in the presence of a novel nano TiO_2 catalyst doped with upconversion luminescence agent *J. Environ. Sci.* **17** 727–30
[12] Qin W, Zhang D, Zhao D, Wang L and Zheng K 2010 Near-infrared photocatalysis based on YF_3:Yb^{3+},Tm^{3+}/TiO_2 core/shell nanoparticles *Chem. Commun.* **46** 2304–6
[13] Shi J, Ye J, Ma L, Ouyang S, Jing D and Guo L 2012 Site-selected doping of upconversion luminescent Er^{3+} into $SrTiO_3$ for visible-light-driven photocatalytic H_2 or O_2 evolution *Chem.-Eur. J.* **18** 7543–51
[14] Chen C K, Chen H M, Chen C-J and Liu R-S 2013 Plasmon-enhanced near-infrared-active materials in photoelectrochemical water splitting *Chem. Commun.* **49** 7917–9
[15] Auzel F 1966 Compteur quantique par transfert d'energie entre de Yb^{3+} a Tm^{3+} dans un tungstate mixte et dans verre germanate *CR Acad. Sci. Paris* B **263** 819–21
[16] Wang F, Deng R, Wang J, Wang Q, Han Y, Zhu H, Chen X and Liu X 2011 Tuning upconversion through energy migration in core–shell nanoparticles *Nat. Mater.* **10** 968–73
[17] Liu Q, Sun Y, Yang T, Feng W, Li C and Li F 2011 Sub-10 nm hexagonal lanthanide-doped $NaLuF_4$ upconversion nanocrystals for sensitive bioimaging *in vivo J. Am. Chem. Soc.* **133** 17122–5
[18] Silver J, Martinez-Rubio M I, Ireland T G, Fern G R and Withnall R 2001 The effect of particle morphology and crystallite size on the upconversion luminescence properties of erbium and ytterbium co-doped yttrium oxide phosphors *J. Phys. Chem.* B **105** 948–53
[19] Wang J *et al* 2014 Enhancing multiphoton upconversion through energy clustering at sublattice level *Nat. Mater.* **13** 157–62
[20] Zhang F, Wan Y, Yu T, Zhang F, Shi Y, Xie S, Li Y, Xu L, Tu B and Zhao D 2007 Uniform nanostructured arrays of sodium rare-Earth fluorides for highly efficient multicolor upconversion luminescence *Angew. Chem. Int. Ed.* **46** 7976–9
[21] Gorris H H and Wolfbeis O S 2013 Photon-upconverting nanoparticles for optical encoding and multiplexing of cells, biomolecules, and microspheres *Angew. Chem. Int. Ed.* **52** 3584–600
[22] Haase M and Schäfer H 2011 Upconverting nanoparticles *Angew. Chem. Int. Ed.* **50** 5808–29
[23] Huang X, Han S, Huang W and Liu X 2013 Enhancing solar cell efficiency: the search for luminescent materials as spectral converters *Chem. Soc. Rev.* **42** 173–201
[24] Ju Q, Tu D, Liu Y, Li R, Zhu H, Chen J, Chen Z, Huang M and Chen X 2011 Amine-functionalized lanthanide-doped $KGdF_4$ nanocrystals as potential optical/magnetic multimodal bioprobes *J. Am. Chem. Soc.* **134** 1323–30
[25] Liu Y, Tu D, Zhu H and Chen X 2013 Lanthanide-doped luminescent nanoprobes: controlled synthesis, optical spectroscopy, and bioapplications *Chem. Soc. Rev.* **42** 6924–58
[26] Wang G, Peng Q and Li Y 2011 Lanthanide-doped nanocrystals: Synthesis, optical-magnetic properties, and applications *Acc. Chem. Res.* **44** 322–32
[27] Zhou J, Liu Z and Li F 2012 Upconversion nanophosphors for small-animal imaging *Chem. Soc. Rev.* **41** 1323–49
[28] Wang F and Liu X 2008 Upconversion multicolor fine-tuning: visible to near-infrared emission from lanthanide-doped $NaYF_4$ nanoparticles *J. Am. Chem. Soc.* **130** 5642–3
[29] Huang P, Zheng W, Zhou S, Tu D, Chen Z, Zhu H, Li R, Ma E, Huang M and Chen X 2014 Lanthanide-doped $LiLuF_4$ upconversion nanoprobes for the detection of disease biomarkers *Angew. Chem. Int. Ed.* **53** 1252–7
[30] Su Q, Han S, Xie X, Zhu H, Chen H, Chen C-K, Liu R-S, Chen X, Wang F and Liu X 2012 The effect of surface coating on energy migration-mediated upconversion *J. Am. Chem. Soc.* **134** 20849–57
[31] Zou W, Visser C, Maduro J A, Pshenichnikov M S and Hummelen J C 2012 Broadband dye-sensitized upconversion of near-infrared light *Nat. Photon.* **6** 560–4
[32] Zhou J, Chen G, Wu E, Bi G, Wu B, Teng Y, Zhou S and Qiu J 2013 Ultrasensitive polarized up-conversion of Tm^{3+}–Yb^{3+} doped β-$NaYF_4$ single nanorod *Nano Lett.* **13** 2241–6
[33] Zhao J *et al* 2013 Single-nanocrystal sensitivity achieved by enhanced upconversion luminescence *Nat. Nanotechnol.* **8** 729–34
[34] Lu Y *et al* 2014 Tunable lifetime multiplexing using luminescent nanocrystals *Nat. Photon.* **8** 32–6

[35] Zhu H, Chen X, Jin L M, Wang Q J, Wang F and Yu S F 2013 Amplified spontaneous emission and lasing from lanthanide-doped up-conversion nanocrystals *ACS nano* **7** 11420–6

[36] Rozo C, Fonseca L F, Jaque D and Solé J G 2008 Photoluminescence of Er-doped Si–SiO_2 and Al–Si–SiO_2 sputtered thin films *J. Lumin.* **128** 897–900

[37] Rozo C, Fonseca L F, Jaque D and García Solé J 2009 Luminescence of Er-doped silicon oxide–zirconia thin films *J. Lumin.* **129** 696–703

[38] Chen H, Yang B, Sun Y, Zhang M, Sui Y, Zhang Z and Cao W 2011 Investigation on upconversion photoluminescence of Bi_3TiNbO_9:Er^{3+}:Yb^{3+} thin films *J. Lumin.* **131** 2574–8

[39] Shusaku A *et al* 2006 Fabrication of optically active Er^{3+}-doped Bi_2O_3–SiO_2 glass thin films by pulsed laser deposition *Jpn. J. Appl. Phys.* **45** 5933

[40] Bubb D M, Cohen D and Qadri S B 2005 Infrared-to-visible upconversion in thin films of $LaEr(MoO_4)_3$ *Appl. Phys. Lett.* **87** 131909

[41] Hao J, Zhang Y and Wei X 2011 Electric-induced enhancement and modulation of upconversion photoluminescence in epitaxial $BaTiO_3$:Yb/Er thin films *Angew. Chem. Int. Ed.* **50** 6876–80

[42] Gurudas U and Bubb D M 2007 Nonlinear optical characterization of $LaEr(MoO_4)_3$ thin films using the Z-scan technique *Appl. Phys.* A **88** 255–9

[43] Zhang X, Serrano C, Daran E, Lahoz F, Lacoste G and Muñoz-Yagüe A 2000 Infrared-laser-induced upconversion from Nd^{3+}: LaF_3 heteroepitaxial layers on CaF_2 (111) substrates by molecular beam epitaxy *Phys. Rev.* B **62** 4446

[44] Satoshi U, Kazunori A, Katsuhiko I, Takafumi Y, Atsuo K and Tsuguo F 1997 High upconversion intensity of Er^{3+} in a LaF_3 thin film on CaF_2 (111) grown by the molecular beam epitaxy method *Jpn. J. Appl. Phys.* **36** L41–4

[45] Que W, Kam C, Zhou Y, Lam Y and Chan Y 2001 Yellow-to-violet upconversion in neodymium oxide nanocrystal/titania/ormosil composite sol–gel thin films derived at low temperature *J. Appl. Phys.* **90** 4865–7

[46] Pang M and Lin J 2005 Growth and optical properties of nanocrystalline $Gd_3Ga_5O_{12}$: Ln powders and thin films via Pechini sol–gel process *J. Cryst. Growth* **284** 262–9

[47] Que W, Liu W and Hu X 2006 Preparation and optical properties of sol–gel neodymium-doped germania/γ-glycidoxypropyltrimethoxysilane organic–inorganic hybrid thin films *Appl. Phys.* B **83** 295–301

[48] Fan W H, Hou X, Zhao W, Gao X J, Zou W and Liu Y 2001 Effect of the growth conditions on infrared upconversion efficiency of CaS: Eu, Sm thin films *Appl. Phys.* A **73** 115–9

[49] Dingemans G, Clark A, van Delft J A, van de Sanden M C M and Kessels W M M 2011 Er^{3+} and Si luminescence of atomic layer deposited Er-doped Al_2O_3 thin films on Si(100) *J. Appl. Phys.* **109** 113107

[50] O'regan B and Grfitzeli M 1991 A low-cost, high-efficiency solar cell based on dye-sensitized *Nature* **353** 737–40

[51] van der Ende B M, Aarts L and Meijerink A 2009 Lanthanide ions as spectral converters for solar cells *Phys. Chem. Chem. Phys.* **11** 11081–95

[52] Yella A, Lee H-W, Tsao H N, Yi C, Chandiran A K, Nazeeruddin M K, Diau E W-G, Yeh C-Y, Zakeeruddin S M and Grätzel M 2011 Porphyrin-sensitized solar cells with cobalt (II/III)-based redox electrolyte exceed 12 percent efficiency *Science* **334** 629–34

[53] Shan G-B, Assaaoudi H and Demopoulos G P 2011 Enhanced performance of dye-sensitized solar cells by utilization of an external, bifunctional layer consisting of uniform β-$NaYF_4$: Er^{3+}/Yb^{3+} nanoplatelets *ACS Appl. Mat. Interfaces* **3** 3239–43

[54] Liang L, Liu Y and Zhao X 2013 Double-shell β-$NaYF_4$: Yb^{3+},Er^{3+}/SiO_2/TiO_2 submicroplates as a scattering and upconverting layer for efficient dye-sensitized solar cells *Chem. Commun.* **49** 3958–60

[55] Ramasamy P and Kim J 2014 Combined plasmonic and upconversion rear reflectors for efficient dye-sensitized solar cells *Chem. Commun.* **50** 879–81

[56] Miao C, Liu T, Zhu Y, Dai Q, Xu W, Xu L, Xu S, Zhao Y and Song H 2013 Super-intense white upconversion emission of Yb_2O_3 polycrystals and its application on luminescence converter of dye-sensitized solar cells *Opt. Lett.* **38** 3340–3

[57] Liu M, Lu Y, Xie Z and Chow G 2011 Enhancing near-infrared solar cell response using upconverting transparentceramics *Sol. Energ. Mat. Sol.* C **95** 800–3

[58] Li Y, Wang G, Pan K, Jiang B, Tian C, Zhou W and Fu H 2012 $NaYF_4$:Er^{3+}/Yb^{3+}–graphene composites: preparation, upconversion luminescence, and application in dye-sensitized solar cells *J. Mater. Chem.* **22** 20381–6

[59] Yu J, Yang Y, Fan R, Zhang H, Li L, Wei L, Shi Y, Pan K and Fu H 2013 Er^{3+} and Yb^{3+} co-doped $TiO_{2-x}F_x$ up-conversion luminescence powder as a light scattering layer with enhanced performance in dye sensitized solar cells *J. Power Sources* **243** 436–43

[60] Richards B S and Shalav A 2007 Enhancing the near-infrared spectral response of silicon optoelectronic devices via up-conversion *IEEE Trans. Electron Devices* **54** 2679–84

[61] Hernández-Rodríguez M A, Imanieh M H, Martín L L and Martín I R 2013 Experimental enhancement of the photocurrent in a solar cell using upconversion process in fluoroindate glasses exciting at 1480 nm *Sol. Energ. Mat. Sol.* **116** 171–5

[62] de Wild J, Meijerink A, Rath J K, van Sark W G J H M and Schropp R E I 2010 Towards upconversion for amorphous silicon solar cells *Sol. Energ. Mat. Sol.* C **94** 1919–22

[63] de Wild J, Rath J K, Meijerink A, van Sark W G J H M and Schropp R E I 2010 Enhanced near-infrared response of a-Si:H solar cells with β-$NaYF_4$:Yb^3+ (18%), Er^3+ (2%) upconversion phosphors *Sol. Energ. Mat. Sol.* C **94** 2395–8

[64] Chen Y, He W, Jiao Y, Wang H, Hao X, Lu J and Yang S-E 2012 β-$NaYF_4$:Er^{3+}(10%) microprisms for the enhancement of α-Si:H solar cell near-infrared responses *J. Lumin.* **132** 2247–50

[65] Li Z Q, Li X D, Liu Q Q, Chen X H, Sun Z, Liu C, Ye X J and Huang S M 2012 Core/shell structured $NaYF_4$: Yb^{3+}/Er^{3+}/Gd^{3+} nanorods with Au nanoparticles or shells for flexible amorphous silicon solar cells *Nanotechnology* **23** 025402

[66] de Wild J, Duindam T F, Rath J K, Meijerink A, van Sark W G J H M and Schropp R E I 2013 Increased upconversion response in a-Si:H solar cells with broad-band light *IEEE J. Photovoltaics* **3** 17–21

[67] Wang H-Q, Stubhan T, Osvet A, Litzov I and Brabec C J 2012 Up-conversion semiconducting MoO_3:Yb/Er nanocomposites as buffer layer in organic solar cells *Sol. Energ. Mat. Sol.* C **105** 196–201

[68] Wu J-L, Chen F-C, Chang S-H, Tan K-S and Tuan H-Y 2012 Upconversion effects on the performance of near-infrared laser-driven polymer photovoltaic devices *Org. Electron.* **13** 2104–8

[69] Lin H-Y, Chen H-N, Wu T-H, Wu C-S, Su Y-K and Chu S-Y 2012 Investigation of green up-conversion behavior in $Y_6W_2O_{15}$:Yb^{3+}, Er^{3+} phosphor and its verification in 973 nm laser-driven GaAs solar cell *J. Am. Ceram. Soc.* **95** 3172–9

[70] Su L T *et al* 2013 Photon upconversion in hetero-nanostructured photoanodes for enhanced near-infrared light harvesting *Adv. Mater.* **25** 1603–7

[71] Liang L, Liu Y, Bu C, Guo K, Sun W, Huang N, Peng T, Sebo B, Pan M and Liu W 2013 Highly uniform,

bifunctional core/double-shell-structured β-$NaYF_4$:Er^{3+}, Yb^{3+}@SiO_2@TiO_2 hexagonal sub-microprisms for high-performance dye-sensitized solar cells *Adv. Mater.* **25** 2174–80

[72] Zhang J, Shen H, Guo W, Wang S, Zhu C, Xue F, Hou J, Su H and Yuan Z 2013 An upconversion $NaYF_4$:Yb^{3+},Er^{3+}/TiO_2 core–shell nanoparticle photoelectrode for improved efficiencies of dye-sensitized solar cells *J. Power Sources* **226** 47–53

[73] Zhou Z, Wang J, Nan F, Bu C, Yu Z, Liu W, Guo S, Hu H and Zhao X-Z 2014 Upconversion induced enhancement of dye-sensitized solar cells based on core–shell structured β-$NaYF_4$:Er^{3+},Yb^{3+}@SiO_2 nanoparticles *Nanoscale* **6** 2052–5

[74] Ciamician G 1912 The photochemistry of the future *Science* **36** 385–94

[75] Fujishima A 1972 Electrochemical photolysis of water at a semiconductor electrode *Nature* **238** 37–8

[76] Pascual J, Camassel J and Mathieu H 1978 Fine structure in the intrinsic absorption edge of TiO_2 *Phys. Rev.* B **18** 5606–14

[77] Turner J A 2004 Sustainable hydrogen production *Science* **305** 972–4

[78] Tang H, Prasad K, Sanjines R, Schmid P and Levy F 1994 Electrical and optical properties of TiO_2 anatase thin films *J. Appl. Phys.* **75** 2042–7

[79] Wang J, Tafen D N, Lewis J P, Hong Z, Manivannan A, Zhi M, Li M and Wu N 2009 Origin of photocatalytic activity of nitrogen-doped TiO_2 nanobelts *J. Am. Chem. Soc.* **131** 12290–7

[80] Wu N, Wang J, Tafen D N, Wang H, Zheng J-G, Lewis J P, Liu X, Leonard S S and Manivannan A 2010 Shape-enhanced photocatalytic activity of single-crystalline anatase TiO_2 (101) nanobelts *J. Am. Chem. Soc.* **132** 6679–85

[81] Thimsen E, Le Formal F, Grätzel M and Warren S C 2010 Influence of plasmonic Au nanoparticles on the photoactivity of Fe_2O_3 electrodes for water splitting *Nano Lett.* **11** 35–343

[82] Yang T-T, Chen W-T, Hsu Y-J, Wei K-H, Lin T-Y and Lin T-W 2010 Interfacial charge carrier dynamics in core–shell Au-CdS nanocrystals *J. Phys. Chem.* C **114** 11414–20

[83] Tian J, Sang Y, Yu G, Jiang H, Mu X and Liu H 2013 A Bi_2WO_6-based hybrid photocatalyst with broad spectrum photocatalytic properties under UV, visible, and near-infrared irradiation *Adv. Mater.* **25** 5075–80

[84] Fagnoni M, Dondi D, Ravelli D and Albini A 2007 Photocatalysis for the formation of the CC bond *Chem. Rev.* **107** 2725–56

[85] Qu Y and Duan X 2013 Progress, challenge and perspective of heterogeneous photocatalysts *Chem. Soc. Rev.* **42** 2568–80

[86] Fujishima A, Rao T N and Tryk D A 2000 Titanium dioxide photocatalysis *J. Photochem. Photobio.* C **1** 1–21

[87] Linsebigler A L, Lu G and Yates J T Jr 1995 Photocatalysis on TiO_2 surfaces: principles, mechanisms, and selected results *Chem. Rev.* **95** 735–58

[88] Asahi R, Morikawa T, Ohwaki T, Aoki K and Taga Y 2001 Visible-light photocatalysis in nitrogen-doped titanium oxides *Science* **293** 269–71

[89] Chen X and Mao S S 2007 Titanium dioxide nanomaterials: synthesis, properties, modifications, and applications *Chem. Rev.* **107** 2891–959

[90] Meng F, Li J, Hong Z, Zhi M, Sakla A, Xiang C and Wu N 2013 Photocatalytic generation of hydrogen with visible-light nitrogen-doped lanthanum titanium oxides *Catal. Today* **199** 48–52

[91] Du J, Lai X, Yang N, Zhai J, Kisailus D, Su F, Wang D and Jiang L 2010 Hierarchically ordered macro–mesoporous TiO_2–Graphene composite films: Improved mass transfer, reduced charge recombination, and their enhanced photocatalytic activities *ACS Nano* **5** 590–6

[92] Zhang M, Chen C, Ma W and Zhao J 2008 Visible-light-induced aerobic oxidation of alcohols in a coupled photocatalytic system of dye-sensitized TiO_2 and TEMPO *Angew. Chem. Int. Ed.* **120** 9876–9

[93] Wang D, Zhao H, Wu N, El Khakani M A and Ma D 2010 Tuning the charge-transfer property of PbS-quantum dot/TiO_2-nanobelt nanohybrids via quantum confinement *J. Phys. Chem. Lett.* **1** 1030–5

[94] Hensel J, Wang G, Li Y and Zhang J Z 2010 Synergistic effect of CdSe quantum dot sensitization and nitrogen doping of TiO_2 nanostructures for photoelectrochemical solar hydrogen generation *Nano Lett.* **10** 478–83

[95] Zhou W, Yin Z, Du Y, Huang X, Zeng Z, Fan Z, Liu H, Wang J and Zhang H 2013 Synthesis of few-layer MoS_2 nanosheet-coated TiO_2 nanobelt heterostructures for enhanced photocatalytic activities *Small* **9** 140–7

[96] Feng G, Liu S, Xiu Z, Zhang Y, Yu J, Chen Y, Wang P and Yu X 2008 Visible light photocatalytic activities of TiO_2 nanocrystals doped with upconversion luminescence agent *J. Phys. Chem.* C **112** 13692–9

[97] Wang F, Wang J and Liu X 2010 Direct evidence of a surface quenching effect on size-dependent luminescence of upconversion nanoparticles *Angew. Chem. Int. Ed.* **122** 7618–22

[98] Wang J, Zhang G, Zhang Z, Zhang X, Zhao G, Wen F, Pan Z, Li Y, Zhang P and Kang P 2006 Investigation on photocatalytic degradation of ethyl violet dyestuff using visible light in the presence of ordinary rutile TiO_2 catalyst doped with upconversion luminescence agent *Water Res.* **40** 2143–50

[99] Wang J, Ma T, Zhang G, Zhang Z, Zhang X, Jiang Y, Zhao G and Zhang P 2007 Preparation of novel nanometer TiO_2 catalyst doped with upconversion luminescence agent and investigation on degradation of acid red B dye using visible light *Catal. Commun.* **8** 607–11

[100] Wang J, Wen F-Y, Zhang Z-H, Zhang X-D, Pan Z-J, Zhang P, Kang P-L, Tong J, Wang L and Xu L 2006 Investigation on degradation of dyestuff wastewater using visible light in the presence of a novel nano TiO_2 catalyst doped with upconversion luminescence agent *J. Photochem. Photobiol.* A **180** 189–95

[101] Wang W, Huang W, Ni Y, Lu C and Xu Z 2013 Different upconversion properties of β-$NaYF_4$:Yb^{3+},Tm^{3+}/Er^{3+} in affecting the near-infrared-driven photocatalytic activity of high-reactive TiO_2 *ACS Appl. Mater. Interfaces* **6** 340–8

[102] Tang Y, Di W, Zhai X, Yang R and Qin W 2013 NIR-responsive photocatalytic activity and mechanism of $NaYF_4$:Yb,Tm@TiO_2 core–shell nanoparticles *ACS Catal.* **3** 405–12

[103] Huang S, Gu L, Miao C, Lou Z, Zhu N, Yuan H and Shan A 2013 Near-infrared photocatalyst of Er^{3+}/Yb^{3+} codoped (CaF_2@TiO_2) nanoparticles with active-core/active-shell structure *J. Mater. Chem.* A **1** 7874–9

[104] Li C, Wang F, Zhu J and Yu J C 2010 $NaYF_4$:Yb,Tm/CdS composite as a novel near-infrared-driven photocatalyst *Appl. Catal. B- Environ.* **100** 433–9

[105] Zhang M, Lin Y, Mullen T J, Lin W-f, Sun L-D, Yan C-H, Patten T E, Wang D and Liu G-y 2012 Improving hematite's solar water splitting efficiency by incorporating rare-Earth upconversion nanomaterials *J. Phys. Chem. Lett.* **3** 3188–92

[106] Li Z-X, Shi F-B, Zhang T, Wu H-S, Sun L-D and Yan C-H 2011 Ytterbium stabilized ordered mesoporous titania for near-infrared photocatalysis *Chem. Commun.* **47** 8109–11

[107] Zhang Y and Hong Z 2013 Synthesis of lanthanide-doped $NaYF_4$@TiO_2 core–shell composites with highly crystalline

and tunable TiO_2 shells under mild conditions and their upconversion-based photocatalysis *Nanoscale* **5** 8930–3
[108] Ren L, Qi X, Liu Y, Huang Z, Wei X, Li J, Yang L and Zhong J 2012 Upconversion-P25-graphene composite as an advanced sunlight driven photocatalytic hybrid material *J. Mater. Chem.* **22** 11765–71
[109] Wang J, Li J, Xie Y, Li C, Han G, Zhang L, Xu R and Zhang X 2010 Investigation on solar photocatalytic degradation of various dyes in the presence of Er^{3+}:$YAlO_3$/ZnO–TiO_2 composite *J. Environ. Manage.* **91** 677–84
[110] Guo X, Di W, Chen C, Liu C, Wang X and Qin W 2014 Enhanced near-infrared photocatalysis of $NaYF_4$:Yb,Tm/CdS/TiO_2 composites *Dalton Trans.* **43** 1048–54
[111] Liu N, Qin W, Qin G, Jiang T and Zhao D 2011 Highly plasmon-enhanced upconversion emissions from Au@β-$NaYF_4$:Yb,Tm hybrid nanostructures *Chem. Commun.* **47** 7671–3
[112] Schietinger S, Aichele T, Wang H-Q, Nann T and Benson O 2009 Plasmon-enhanced upconversion in single $NaYF_4$:Yb^{3+}/Er^{3+} codoped nanocrystals *Nano Lett.* **10** 134–8
[113] Johnson C M, Reece P J and Conibeer G J 2011 Slow-light-enhanced upconversion for photovoltaic applications in one-dimensional photonic crystals *Opt. Lett.* **36** 3990–2
[114] Sun Q-C, Mundoor H, Ribot J C, Singh V, Smalyukh I I and Nagpal P 2014 Plasmon-enhanced energy transfer for improved upconversion of infrared radiation in doped-lanthanide nanocrystals *Nano Lett.* **14** 101–6
[115] Xie X, Gao N, Deng R, Sun Q, Xu Q-H and Liu X 2013 Mechanistic investigation of photon upconversion in Nd^{3+}-sensitized core-shell nanoparticles *J. Am. Chem. Soc.* **135** 12608–11
[116] Xie X and Liu X 2012 Photonics: upconversion goes broadband *Nat. Mater.* **11** 842–3
[117] Gai S, Li C, Yang P and Lin J 2013 Recent progress in rare Earth micro/nanocrystals: soft chemical synthesis, luminescent properties, and biomedical applications *Chem. Rev.* **114** 2343–89
[118] Wang S, Feng J, Song S and Zhang H 2013 Rare Earth fluorides upconversion nanophosphors: from synthesis to applications in bioimaging *CrystEngComm* **15** 7142–51